arXiv:1801.06223v1 [astro-ph.SR] 18 Jan 2018

Effect of Supernovae on the Local Interstellar Material

Priscilla Frisch and Vikram V. Dwarkadas

Abstract A range of astronomical data indicates that ancient supernovae created the galactic environment of the Sun and sculpted the physical properties of the interstellar medium near the heliosphere. In this paper we review the characteristics of the local interstellar medium that have been affected by supernovae. The kinematics, magnetic field, elemental abundances, and configuration of the nearest interstellar material support the view that the Sun is at the edge of the Loop I superbubble, which has merged into the low density Local Bubble. The energy source for the higher temperature X-ray emitting plasma pervading the Local Bubble is uncertain. Winds from massive stars and nearby supernovae, perhaps from the Sco-Cen Association, may have contributed radioisotopes found in the geologic record and galactic cosmic ray population. Nested supernova shells in the Orion and Sco-Cen regions suggest spatially distinct sites of episodic star formation. The heliosphere properties vary with the pressure of the surrounding interstellar cloud. A nearby supernova would modify this pressure equilibrium and thereby severely disrupt the heliosphere as well as the local interstellar medium.

Priscilla Frisch
University of Chicago, Department of Astronomy and Astrophysics, 5640 S Ellis Ave, Chicago, IL 60637, e-mail: frisch@oddjob.uchicago.edu

Vikram V. Dwarkadas
University of Chicago, Department of Astronomy and Astrophysics, 5640 S Ellis Ave, Chicago, IL 60637, e-mail: vikram@oddjob.uchicago.edu

Contents

Effect of Supernovae on the Local Interstellar Material 1
Priscilla Frisch and Vikram V. Dwarkadas
1 Introduction 2
2 Gould's Belt and Massive Stars 3
3 Supernova Remix of the Interstellar Medium 5
3.1 Bubbles and Superbubbles 6
3.2 Radio Superbubbles and Magnetic Loops 7
3.3 The Local Bubble 9
3.4 Loop I and the Very Local Interstellar Medium 10
3.5 Line-of-sight Blending of Loop I and Loop IV with Galactic Center Backgrounds 13
3.6 The Orion-Eridanus Superbubble 14
4 Isotopic and Abundance Indicators of SN Activity 16
4.1 ^{60}Fe radioisotope Observations as Indicators of Nearby Supernovae 16
4.2 Isotopes and the OB Association Origin of Galactic Cosmic Rays 18
4.3 ^{26}Al as a Tracer of Massive Stars 19
5 Impact of Supernova on Heliosphere 20
6 Conclusions 22
References 23

1 Introduction

Nearly a century ago Harlow Shapley [1] noticed that the Sun is traveling away from Orion and speculated that variations in the brightness of Orion stars could result from encounters between the stars and nebulosity that would "gravely affect the atmosphere surrounding any attendant planet". By analogy he suggested that were the Sun to encounter diffuse nebulosity it could induce severe changes in the terrestrial

climate. Such an idea is not far-fetched. Supernovae and winds from massive stars inject large amounts of energy into the interstellar medium and reshape and remix interstellar material with shock waves and expanding bubbles. Nearby supernovae occur at rates that are larger than the galactic average due to the solar location inside of Gould's Belt. The flux of galactic cosmic rays into the terrestrial atmosphere depends on the response of the heliosphere to the ambient interstellar medium [2, 3]. Geologic records indicate that cosmic rays from supernova have penetrated to the surface of the Earth [4]. The Sun is traveling toward the constellation of Hercules at a velocity of ~ 18 pc per Myr through the local standard of rest (LSR) [5]. Without question the supernovae that generated the Loop I superbubble [6] affected the ambient interstellar medium and possibly the interplanetary environment of the Earth. Locations of many supernovae within 400 pc and over the past ~ 2 Myr have been identified.

The Sun is immersed in a small (< 15 pc) cluster of low density partially ionized interstellar cloudlets of the type that were once identified as the "intercloud medium" because of the low extinctions, E(B-V)< 0.001 mag. Most local gas is warm, $T = 5000 - 12,500$ K, low density partially ionized gas with log N(HI)< 18.7 cm^{-2}, $<n_{HI}>= 0.01 - 0.10$ cm^{-3}, and $n_p \sim 0.1$ cm^{-3} (e.g. [7, 8, 9]). A magnetic field with strength ~ 3 μG shapes the heliosphere [10, 11]. The only known local cloudlet that is cold and neutral is the filamentary Local Leo Cold Cloud (LLCC) dust cloud at distance ~ 18 pc [12, 13].

This review discusses the configuration of massive stars in Gould's Belt that spawn nearby supernovae (Section 2), bubble formation (Section 3.1), the location of the Sun inside a superbubble rim (Section 3.4) that merges into the low density Local Bubble cavity (Section 3.3), the Orion superbubble (Section 3.6), short-lived radioisotope clocks of recent nearby supernova found in geological and astrophysical data (Section 4), and the impact of supernovae on the heliosphere (Section 5).

The Local Bubble is characterized by a cavity in the interstellar medium (ISM). Figure 1 shows the distribution of interstellar material within ~ 400 pc according to the cumulative reddening of starlight as measured by the color excess E(B-V) (Frisch et al. 2015,[5], in preparation). Superimposed on the reddening maps are nearby superbubble shells, the interarm interstellar magnetic field (ISMF) indicated by pulsar data [14], and the local ISMF direction diagnosed by the Ribbon of energetic neutral atoms (ENAs) discovered by the Interstellar Boundary Explorer (IBEX) spacecraft [15, 16, 17, 18, 19]. The extinction void around the Sun, denoted the Local Bubble, occurs where the interior of Gould's Belt blends into the interarm regions of the third galactic quadrant.

2 Gould's Belt and Massive Stars

Nearby clusters of O–B2.5 massive stars that are progenitors of core-collapse Type II and Type Ib/c supernovae form a thin planar ring-like structure around the Sun known as "Gould's Belt" [21, 22, 23]. Gould's Belt is part of a large-scale warp in

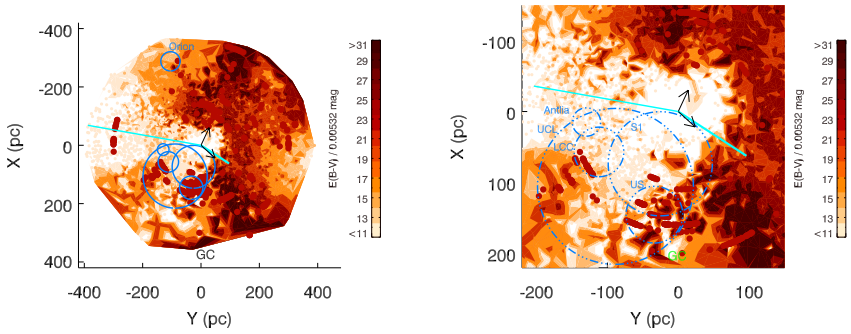


Fig. 1 The Local Bubble: The cumulative extinction of interstellar dust is shown over spatial scales of $\sim$ 300 pc (right) and $\sim$ 800 pc (left) projected onto the galactic plane (from [20]). The galactic center is at large positive values of X and the galaxy rotates toward positive Y values. The cumulative extinction is determined from the color excess E(B-V) measured for each star where the astrometric distances are required to agree with distances obtained from E(B-V) and the spectral type of the star (see Frisch et al., 2015, [5] for more information). The color bar shows color excess E(B-V) in units of 0.00532 mag. Round dark maroon circles show the locations of nearby molecular CO clouds. The two black arrows show the LSR velocities of the CLIC (perpendicular to the S1 shell) and the Sun (roughly tangential to the S1 shell). The long and short cyan-colored lines show the directions of the interarm magnetic field and IBEX Ribbon magnetic field directions, respectively [17, 5]. The circles show the three superbubble shells in Sco OB2, the Antlia SN remnant, and the Ori-Eri superbubble (left figure only), and the S1 shell (see text for details).

the distribution of young stars in the galactic plane [24]. The traditional configuration of Gould's Belt as an inclined plane defined partly by the Sco OB2 and Orion OB1 associations is shown in Figure 2 (from Grenier 2004, [22]). Gould's belt is tilted by an angle of $\sim 17.2^\circ$ with respect to the galactic plane, with the ascending node toward $\sim 296^\circ$, and centered ~ 104 pc away toward $\ell \sim 184^\circ$, where the uncertainties arise from the different selection criteria for testing the Gould's Belt configuration [25, 21, 22, 26]). An alternate perspective compares the distribution and kinematics of open clusters in the Orion OB1 association with those of Sco OB2 to characterize Orion OB1 as belonging to the Local Arm where high densities of open clusters and ongoing star formation appear, in contrast to the Sco OB2 stars that are located on the outskirts of the Local Arm with lower densities of active star-forming regions [27, 28]. Elias et al. [28] establish that the Local Bubble region around the Sun is devoid of open clusters in comparison to the Orion region. Bobylev and Bajkova (2014, [26]) used astrometric data to define the Orion arm as a narrow ellipsoid directed toward $\ell = 77.1^\circ \pm 2.9^\circ$ with a symmetry plane inclined to the Galactic plane by $5.6^\circ \pm 0.2^\circ$, and with a longitude of the ascending node of the plane toward $70^\circ \pm 3^\circ$ [26]. Regardless of the detailed description of Gould's

Belt versus the Local Arm, most of the early-type O–B2.5 massive stars in the solar vicinity coincide with the traditional configuration of Gould's Belt.

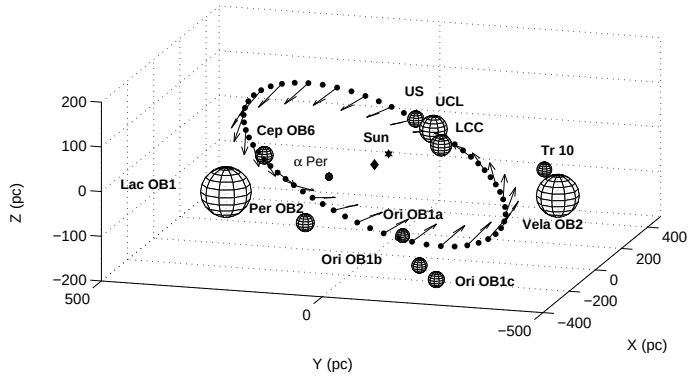


Fig. 2 Gould's Belt: Stellar associations of Gould's Belt and the velocity field of the stars with respect to the LSR are shown in 3D. The diamond shows the center of Gould's Belt and the star shows the location of the Sun. The galactic center is directed toward large positive values for the x-coordinate. Figure from Grenier (2004, [22]).

About 17–20 supernovae per million years formed in the entire Gould's Belt during the past several million years, which is a rate 3–4 times that of the local galactic average [22]. Since 80% of galactic supernova are from the core collapse of massive stars, the SNe in Gould's Belt will account for the most likely supernova to have shaped the physical properties of the local interstellar medium. Over tens of millions of years these supernovae have rearranged the interstellar material near the Sun into the networks of filaments, arcs, shells and superbubbles that are observed [29, 30, 31].

3 Supernova Remix of the Interstellar Medium

Superbubble shells, either complete, or incomplete "worm" or filamentary structures, are common in the ISM and are nearly all explained by energy injection from stellar winds and supernovae (Heiles 1984, [30]). Measurements of the Zeeman splitting of the HI 21-cm line shows that morphologically distinct filaments generally consist of warm neutral or partially ionized gas where magnetic pressure dominates thermal pressures by a factor of ~ 67, and turbulent pressure by a factor of ~ 10 [32]. The rapid evolution of massive stars in Gould's Belt has frequently altered the ISM in the solar neighborhood.

3.1 Bubbles and Superbubbles

Supersonic winds from massive stars can evacuate large regions of space around the star, with radii of several parsecs. The detailed structure of these 'wind-blown bubbles' was first elucidated by Castor et al. (1975, [33]) and Weaver et al. (1977, [34]), and has been subsequently refined and discussed by many authors [35, 36, 37]. In general, the bubbles consist of a very low density (< 0.01 particles cm^{-3} on average) interior surrounded by a dense shell of material, bounded by a radiative shock that serves as the boundary of the bubble. The bubbles can be either density or ionization bounded - if the shell is dense enough, an ionization front will be trapped in the dense shell, beyond which neutral material can be found. The ISM magnetic field can also affect the size, shape and evolution of circumstellar bubbles [38]. Weaver et al. (1977, [34]) showed that the radius of the bubbles primarily grows with time as $R_b \propto \left[\frac{L}{\rho}\right]^{1/5} t^{3/5}$ where $L = 0.5\dot{M}v_w^2$ is the mechanical luminosity of the wind with mass-loss rate $\dot{M}$ and wind velocity v_w, and ρ is the density of the ambient medium.

Numerical simulations have been successful in confirming the analytical predictions and reproducing the general structure, formation and morphology of massive-star bubbles [39, 40, 41, 42, 43]. Other simulations have explored the evolution of the subsequent supernova shock waves within the bubbles [44, 45, 46, 47, 43, 48]. Although the highly supersonic winds around massive stars (wind velocity on order 1000-2000 km s^{-1}), and the low density and high pressure pervading the bubble would point to an extremely high temperature within the bulk of the bubble (of order 10^7 to 10^8 K), X-ray observations have shown that if hot gas is detected at all, its temperature and emission measure are both low, on the order of a few times 10^6 K [49, 50, 51, 52]. Many authors have tried to simulate these observations to understand the origin of the low temperatures, with some degree of success in matching the bubble temperatures and their X-ray spectra [53, 54, 55].

Clusters of massive stars group together to form an association. The correlated supernovae resulting from the explosion of these stars can form even larger bubbles due to the combined effects of the winds and supernova explosions. The aptly named superbubbles [56, 57, 58] rearrange the morphology and physical characteristics of the surrounding ISM. Heiles (1979, [29]) defines bubbles with injected energies greater than 3×10^{52} ergs as supershells or superbubbles. The structure of these superbubbles is similar to their smaller brethren, and can be approximated from the bubble theory allowing for continuous energy input from an association of stars and their resulting SNe. MacLow and McCray (1988, [56]) have shown that the bubble approximation is valid even for superbubbles, and show that the superbubble radius can be written as $R_{sb} \sim 267 \left[\frac{L_{38} t_7^3}{n_0}\right]^{1/5}$ pc, where L_{38} is the mechanical luminosity in terms of 10^{38} ergs s^{-1}, t_7 is the time in units of 10^7 years, and n_0 is the atomic number density. Due to their extremely large size, it is clear that these bubbles are not expanding in a homogeneous interstellar medium but in a medium

whose structure is constantly being stirred due to heating by supernova explosions [59].

The expanding flow sweeps up interstellar material and magnetic fields into a postshock shell. The mass within the bubble interior is likely regulated by evaporation from the cool bubble walls, by entrainment and ablation from denser clouds remaining within the bubble, and by the penetration of ambient interstellar clouds that are not destroyed by the photoevaporative effect of the massive star [60, 61]. A superbubble shell thickens as it sweeps up magnetic field lines during the pressure-driven snowplow stage, producing regions in the evolved shell where the ISMF is perpendicular to the gas velocity [62, 63, 64], such as is found for the immediate solar environment (Section 3.4). For a cylindrical model with the ISMF parallel to the axis of the cylinder, superbubble expansion parallel to the radial direction produces a configuration where gas velocities are perpendicular to the ISMF direction [63].

It is in the context of these known bubbles that superbubbles in our vicinity, and the detection of a low density, high temperature region around our solar system, the Local Bubble, need to be evaluated.

3.2 Radio Superbubbles and Magnetic Loops

The closest superbubbles that have influenced the local ISM occurred in the Sco-Cen association, and were first revealed through observations of the intense radio continuum source known as the North Polar Spur (NPS) that extends north from longitude $\ell \sim 30^\circ$. The NPS was part of a loop-like structure with a non-thermal continuum, that was modeled as a supernova remnant likely to be within 100 pc [65, 66]. Berkhuijsen et al. (1971, [67, 6]) identified four non-thermal radio loops at 830 MHz, Loops I–IV, with the NPS the brightest part of Loop I (see early review by Salter,1983, [68]). The strongly polarized radio Loop I (64% to 72% polarization), indicates a magnetic field that is uniform in direction [69]. Loops II and III are radio-continuum features [67, 70] while Loop IV coincides with the extended HII region around the nearby B1V star Spica indicating that Loop IV does not have a supernova origin [71]. Using skymaps from the Wilkinson Microwave Anisotropy Probe (WMAP) at 23, 33, and 41 GHz, Vidal et al. [72] identified the original four loops and eleven new non-thermal loop structures, some prominent only through polarization. The mean spectral index for the brightness temperature of the polarized emissions is -3.06 ± 0.02, verifying the synchrotron nature of the emission from these radio loops.

Filling in the picture of the influence of supernova on the local ISM requires data on the neutral ISM. Heiles [29] identified sixteen stationary HI shells within 500 pc that have diameters $\leq 36^\circ$. Eleven large interstellar shells beyond 500 pc were termed “supershells”. Radio-recombination lines showed that warm, 7000 K, partially ionized filamentary structures are common throughout the ISM [76].

The largest diameter radio bubble in the sky is Loop I. Successive epochs of star formation in the parent molecular cloud of Sco OB2 created large-scale nested

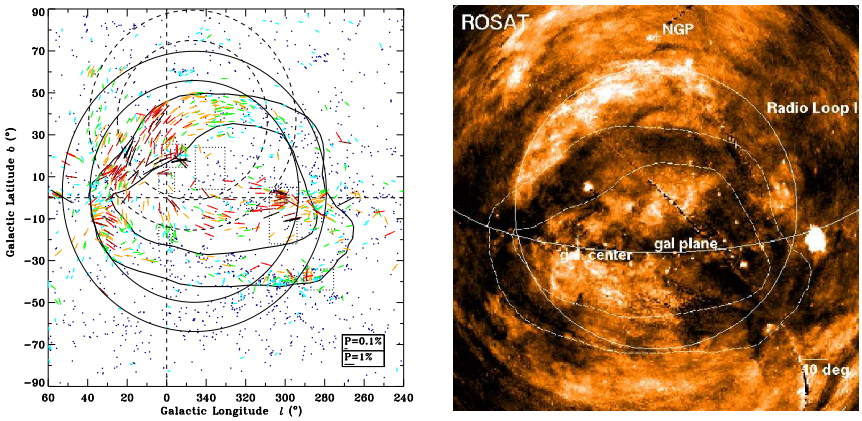


Fig. 3 Left: Polarized starlight toward Loop I: The optical polarizations that trace the ISMF in the neutral gas that shadows the soft X-ray background (right) are shown together with the S1/S2 superbubble shells (solid/dashed circles respectively) from Wolleben (2007, [73]). The irregular lines reproduce the boundaries of the "interaction ring" shown at right. Figure from Santos et al. 2011, [74]. Right: Egger interaction ring: Soft X-ray shadow appearing in ROSAT data in the energy range 0.1–2.0 keV. The X-ray shadow is caused by neutral gas with a density of ~ 15 cm^{-3}, and aligned dust grains that polarized background starlight. between two interstellar bubbles. Also identified are the location of Loop I (solid white line), the interaction ring between the Local Bubble plasma and the Loop I bubble (outlined by dashed lines), and galactic landmarks. The X-ray shadow corresponds to column densities that jump from N(H)$\sim 10^{20}$ cm^{-2} to 7×10^{20} cm^{-2}. Optical and UV data indicate a neutral wall with N(H)$\sim 10^{20}$ cm^{-2} at a distance of 40 ± 25 pc. Figure from Egger and Aschenbach 1995, [75], and courtesy of the Max-Planck-Institut fur extraterrestrische Physik (http://www/mpi/mpg/de/).

interstellar HI shells that have provided the basis for linking nearby bubble-like structures, such as Loop I, with the parent clusters of stars [77, 78]. Polarization data suggest these nested shells are closer to the Sun, (at a distance ~ 100 pc), in the region $20^\circ < \ell < 40^\circ$ than in the region $290^\circ < \ell < 310^\circ$ where distances are > 200 pc [74]. The three subgroups of the Scorpius-Centaurus Association [79] are the Upper Centaurus-Lupus (UCL), Lower Centaurus Crux (LCC), and Upper Scorpius (US). Their nuclear ages were thought to be 14–15 Myr, 11–12 Myr and 4–5 Myr respectively (deGeus 1992, [80], see Figure 1). However, recent re-examination of the evolutionary state and isochronal ages data by [81] and [82] suggests that the subgroups are not consistent with being simple, coeval populations which formed in single bursts, but likely represents a multitude of smaller star formation episodes of hundreds to tens of stars each. They have also re-evaluated the ages and find them to be higher, at 16 Myr (UCL), 17 Myr (LCC) and $11 \pm 1 \pm 2$ Myr (statistical, systematic) for US. The US age is twice as large as previously assumed. When stellar proper motions are included, it is seen that the shell-forming events did not occur at the present locations of the stellar subgroups, and the LCC is the most likely source of the large-scale Loop I feature [83]. Frisch (1981, [84]) pointed out that

the low density interarm-type material near the Sun would have led to asymmetric expansion of Loop I. The X-ray remnant toward the NPS would have resulted from star formation triggered by the impact of a shock wave on the Aquila Rift dark cloud [78, 77, 80]. Iwan [85] found that a reheated supernova remnant was required to simultaneously explain the Loop I HI radio shell and the ridge of X-ray plasma, although she could not incorporate the then-unknown foreground contamination of the X-ray background by solar wind charge-exchange with interstellar neutrals [86].

3.3 The Local Bubble

The discovery of the soft X-ray background (SXRB, [92]) motivated measurements of the X-ray spectra at low energies, < 2.5 keV, where a flat X-ray spectrum was found that limited the amount of possible interstellar absorption of the X-ray photons [93]. The resulting "displacement model" required the X-rays to be produced inside a cavity in the neutral gas [94, 95]). The original interpretation of the SXRB data as tracing an evolved supernova remnant has been reviewed in [96, 97]. Interpreting the physics of the hot gas has been surprisingly difficult because the local source of the hot plasma could not be identified. The supernova explosion that produced the Geminga pulsar was initially suggested to account for the soft X-ray emission [98], but Geminga was shown to originate near Orion instead [99, 100, 101]. It is now known that the low energy X-ray spectrum is contaminated by foreground emission from charge-exchange between solar wind plasma and interstellar neutrals [86].

It had been suggested by Cox and Smith (1974, [102]) that supernovae could form and maintain a mesh of interconnected tunnels of low density high temperature gas in the interstellar medium, producing structures similar to the Local Bubble. Frisch (1981, [84]) argued that the data indicated that the local interstellar medium had been processed by a shock front at least 2 Myr ago based on age limits set by the soft X-ray emissions and deep sea sediments containing Be^{10}, and suggested that it could be an extension of the Loop I or North Polar Spur seen in the Scorpius-Ophiucus region. In the opposite direction one study predicts that the supernova forming the Antlia remnant exploded 1.20 Myr ago and 128 pc away at $\ell = 270.4,\ b = 19.2^{\circ}$ [103]. Smith and Cox (2001, [104]) have shown that multiple SNe within about 3 Myr can produce a bubble with conditions that resemble the Local Bubble. However a model where a homogeneous local plasma at temperatures $\sim 10^6$ K accounts for all of the low energy X-ray emission has been elusive, as discussed in detail by Welsh and Shelton (2009, [105]).

No signs of a cluster of massive stars interior to the Local Bubble have been found. Using a kinematic analysis of the entire solar neighborhood within about 400 pc, Fuchs et al. (2006, [106]) have suggested that the youngest associations in the solar neighborhood entered the present bubble region about 10-15 Myr ago, and that approximately 14-20 have exploded since then, a view consistent with the earlier studies of Maiz-Apellaniz (2001, [83]). With the help of non-equilibrium ionization

modeling, de Avillez and Breitschwerdt [107] have constrained the evolution time since the last SN to be about 0.5-0.8 Myr. These parameters are in rough agreement with those derived from ^{60}Fe (see Section 4.1).

Charge exchange (CEX) between the solar wind ions and interstellar atoms has been suggested as at least a partial, if not complete, source for the diffuse X-ray background by Cravens et al. (2001, [108]). The origin of foreground contamination near 0.75 keV and 0.25 keV differ, with the former primarily due to CEX with solar wind oxygen atoms and the latter due to CEX with L-shell states for many species for which transition strengths are unknown [109]. Predictions of foreground CEX emission in the 0.75 keV band yield a hard spectrum and does not predict the CEX rates required to discount an interstellar source of the SXRB [110, 105]. At lower energies, X-ray shadows are seen in the 0.094 keV Wisconsin band. The best models of simultaneous solar wind foreground and a thermal Local Bubble hot plasma indicate that the Local Bubble produces produces $26\% \pm 4\%$ of the 0.1–0.4 keV emissions [111]. An alternative analysis finds solar wind charge exchange foreground levels of 43% to 76% of the SXRB produced by the Local Bubble in the 0.25 keV ROSAT band in the direction of the local cold Leo cloud [112, 113]. These results seem to reaffirm that the Local Bubble cavity is filled with a uniform hot gas, but also indicate that more efforts to understand the foreground are needed.

The properties of the Local Bubble, and the similarity to other (super)bubbles, coupled with the general observations of a 3-phase interstellar medium with a hot phase consisting of low density, high temperature gas [31], hint at a massive star and/or supernova origin. Other evidence within the Local Bubble also points towards a SN origin. [114] and [115] study the peculiar characteristics of a cometary-shaped infrared cirrus cloud towards the star HD 102065. The interpretation attributes the spatial structure in the cold phase, the high (and negative) velocities, the high abundance of atoms in excited states, a high level of ionization associated with the highest velocities, as well as the unusually high abundance of small dust particles, as all due to the interaction of the molecular cloud with a SN shock wave approximately 200,000 to 300,000 years ago.

3.4 Loop I and the Very Local Interstellar Medium

The physical characteristics of the nearest interstellar material, including the geometry of Loop I, local cloud kinematics, interstellar magnetic field, and gas-phase abundances, indicate an origin for the cluster of local interstellar clouds (CLIC) within ~ 15 pc that is related to the Loop I superbubble. An alternate origin for the CLIC as a magnetic flux tube that detached from the Local Bubble walls (Cox and Helenius, 2003 [116]) has not yet been tested against recent data. The CLIC contains kinematically defined interstellar clouds that are located mainly within 15 pc of the Sun (Figure 4). The result that the Sun is in the rim of the Loop I superbubble rests on several arguments.

Geometrical considerations: Studies of the Loop I geometry consistently place the Sun in or close to the rim of the Loop I bubble if it is spherical. Models of radio Loop I and the NPS as a single shell yield a shell center at $\ell = 325^\circ$, $b = 17.5^\circ$, and 130 ± 75 pc with a diameter of 230 ± 135 pc [67, 6, 117, 118]. Wolleben (2007,[73]) fit two separate spherical superbubble shells, S1 and S2, to the polarized Loop I radio continuum emission using a model of a spherical superbubble shell expanding in a uniform magnetic field ([119], Fig. 1, Fig. 3, left). The Sun is located in the rim of the S1 shell that is centered at $\ell \sim 346^\circ$ and distance 78 ± 10 pc, with the distance comparable to the shell radius (62–101 pc). The HI 21-cm shell of Loop I is centered at at $\ell = 320^\circ$, $b = 5^\circ$, and has a distance and radius of ~ 118 pc [120].

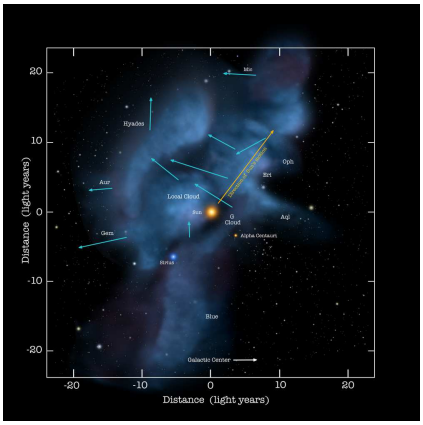


Fig. 4 Nearby clouds: Locations of the tenuous local interstellar clouds within ~ 15 pc are shown projected onto the galactic plane, together with the cloud motions through the LSR (blue arrows, [121]). Names are shown for the clouds [122] and several nearby stars. The solar apex motion through the LSR is marked with the yellow arrow. The center of the S1 shell is about 78 pc beyond α Cen. Figure credit: NASA, Adler Planetarium, P. C. Frisch, S. Redfield.

CLIC kinematics: The upwind direction of the bulk motion of the CLIC through the LSR is directed toward the center of Loop I, indicating that the Sun is in the Loop I shell that is still expanding at a velocity of 17.3 km s^{-1} [5]. The kinematics of the low density interstellar gas within 15 pc have been evaluated using two different assumptions; as a coherent flow of interstellar gas and dust through space [123, 124, 125, 126, 127], or as a group of separate cloudlets with different velocities [128, 129, 130, 126, 131, 122]. Cloud velocities are found from interstellar absorption lines (e.g. [128, 7]). Velocities for the cloud around the heliosphere can also be estimated from in situ measurements of interstellar gas (e.g. [132, 133]) and dust [134, 135] that share similar velocities. The upwind direction of the CLIC interstellar wind [5] coincides with the center of the S1 shell [73], with an angle of $14^\circ \pm 18^\circ$ between CLIC LSR velocity and the S1 shell center. The flow of local interstellar gas away from the Loop I region was discovered decades ago [136, 84, 123, 124, 125] and recent fits to different selections of interstellar absorption line data lead to similar

results for the bulk flow; note that the vector directions in Gry and Jenkins (2014, [127]) and Frisch et al. (2002, [126]) differ by $11^\circ \pm 17^\circ$.

Perpendicular relation between interstellar magnetic field direction and LSR cloud velocities: Swept-up field lines near the equator of an expanding superbubble shell are perpendicular to the expansion velocity [62, 63]. Wolleben [73] assumed such a configuration when evaluating the geometry of the S1 and S2 shells. This property gives cloud velocities that are perpendicular to the ISMF for the equatorial regions of the bubble. The bulk velocity of the CLIC through the LSR is perpendicular to the CLIC ISMF direction, and the LSR vector of the Local Interstellar Cloud (LIC) gas that surrounds the heliosphere is perpendicular to the LIC magnetic field direction. The angle between the bulk CLIC velocity and the interstellar magnetic field direction determined from polarized light from nearby stars is $80^\circ \pm 8^\circ$ [9, 5]. The ISMF direction is obtained from the statistical analysis of polarized starlight, giving an ISMF pole toward $\ell = 36.2^\circ,\ b = 49.0^\circ\ (\pm 16^\circ)$ [5], where the polarization is caused by the attenuation of starlight by a dichroic screen of foreground dust grains aligned with respect to the ISMF [137]. The LIC magnetic field direction is found from the center of the IBEX ribbon arc of higher ENA fluxes, $\ell = 34.8^\circ \pm 4.3^\circ$, $b = 56.6^\circ \pm 1.2^\circ$, which forms upwind of the heliopause where the ISMF draping over the heliosphere becomes perpendicular to the sightline [15, 16, 19]. The velocity of the LIC gas has been determined from IBEX in situ measurements of neutral interstellar He, H, and O flowing through the heliosphere [140, 155, 141, 142] and corresponds to a LIC LSR velocity of 17.2 ± 1.9 km s^{-1} toward $\ell = 141.1^\circ \pm 5.9^\circ,\ b = 2.4^\circ \pm 4.2^\circ$ [5]. The LIC ISMF direction and LSR velocity are nearly perpendicular, with an enclosed angle of $87.6^\circ \pm 3.0^\circ$ [155]. The ISMF directions in the CLIC and LIC agree to within $7.6^{+14.9}_{-7.6}$ degrees [5].

Local ISMF orders kinematics of local clouds: An alternate view of CLIC kinematics is provided by parsing the observed velocity components into individual cloudlets. A self-consistent analysis of separate cloud velocities has been developed by Redfield and Linsky (2008, [122]). Comparisons between the LSR velocities of these clouds [121] and the IBEX ISMF direction [17, 5] reveal that the LSR cloud velocities are roughly proportional to the angle between the LSR cloud velocity vector and the ISMF direction (see Figure 12 of Frisch et al. (2015, [5]).

Abundance pattern of gas-phase elements: Clear evidence that the local ISM has been processed by passage through supernova shocks is provided by comparisons between the abundance patterns of interstellar gas and solar abundances. Elements missing from the gas are due to the condensation of minerals onto dust grains [143]. Frisch [84] and Crutcher [123] attributed the relatively high abundances of refractory elements in nearby interstellar gas to the erosion of grains by shocks originating in the Sco-Cen Association. Early data on Ca II and Na I gas-phase abundances found that the abundances of Ca II and other refractory elements increased with the cloud LSR velocity [144, 145, 146] because of the processing of interstellar dust in high-temperature shocks that erode the refractory component of the grains (e.g. [147, 148, 110, 149]. Interstellar depletions for 243 sightlines (Jenkins 2009, [150]) have been characterized by considering the common parameter that describes the depletion pattern as a function of element, and a second parameter that describes

depletion patterns between sightlines. Interstellar depletions increase with the total hydrogen column density, but unrecognized ionization of the gas will produce inaccurate weaker depletions of refractory elements such as Fe^+ and Mg^+ that have low first ionization potentials. The abundance patterns in the CLIC gas are similar to those of warm clouds [151] but vary between individual cloudlets [122]. The velocities of LIC gas [133] and LIC dust (from in situ measurements of interstellar dust inside of the heliosphere [134, 135]) are in agreement indicating that the grain destruction must have occurred far in the past.

The best constrained interstellar cloud, the LIC, has an origin in a superbubble shell: The best understood interstellar cloud is the LIC that feeds interstellar gas [110, 9, 152] and dust [134, 135, 153, 154] into the heliosphere, and is detected toward over 75 stars [122]. IBEX data permit the detailed study of the LIC at one spatial location; those data show that the LIC LSR velocity and LIC ISMF directions are perpendicular and the upwind direction of the LIC velocity is toward the center of Loop I [155, 142, 5]. Abundances in the LIC have been corrected for ionization effects using self-consistent radiative transfer models [10]. Components of the models include a source of EUV photons to account for high ratios of HI/HeI found in pickup ion and anomalous cosmic ray data inside of the heliosphere [156, 157, 158, 159], and toward nearby white dwarf stars [160, 161]. Pickup ions and anomalous cosmic rays form from interstellar neutrals that survive penetration into the heliosphere [162] and are either directly sampled through in situ measurements [15, 140, 163, 141, 142, 164, 165] or ionized through charge-exchange, photoionization, and other processes [162] to create the pickup ion population [156, 157] or accelerated to become the anomalous cosmic ray population [159]. Using LIC data toward ε CMa and pickup ion and in situ heliospheric data, elemental abundances have been reconstructed for the LIC [166, 167, 10]. Predictions from these models include densities of $n_{HI} \sim 0.19$ cm^{-3}, n(e)~ 0.07 cm^{-3}, ionization levels of hydrogen and helium $\sim 22\%$ and $\sim 39\%$ respectively for a cloud temperature of 6300 K, the full destruction of carbonaceous grains in the LIC, and elevated gas-phase abundances for Fe and Mg that indicate silicate grains [10]. In situ measurements of interstellar HeI inside of the heliosphere yield a LIC temperature of 8000 ± 1300 K [133]. Solar abundances are also found for carbon in the low density gas at intermediate and high velocities toward Orion [168, 151]. The LIC abundance pattern fits into the interstellar abundance patterns that depend on cloud velocity, which are nicely established for the low-velocity, intermediate velocity, and high-velocity clouds studied towards towards Orion where different clouds have been shocked differently (Welty et al. 1999, 2002, [151, 168]).

3.5 Line-of-sight Blending of Loop I and Loop IV with Galactic Center Backgrounds

Several recent studies [87, 88] have attributed X-ray features toward Loop I to the gamma-ray bubbles around the galactic center found by Fermi-Lat [89]. This hy-

pothesis requires that the Fermi-bubbles extend over 5 kpc into the galactic halo. The arguments for a galactic center origin of Loops I and IV rely partly on the latitude dependence of the North Polar Spur X-ray emission compared to that of dust, HI or molecular material. The North Polar Spur was originally defined as an intense source of non-thermal radio continuum, and subsequently associated with Loop I and found be a strong source of X-ray emission. While distant contributions to the North Polar Spur soft X-ray emission can not be ruled out, especially given the complex spectrum for the NPS X-ray emission at ~ 0.15 keV suggestive of a reheated supernova remnant [85], studies of polarized stars with known distances clearly prove that the main radio continuum Loop I is a local phenomena within ~ 200 pc [74, 90]. Faraday tomography of the radio continuum adjacent to the North Polar Spur region indicates that radio emission from the spur is not Faraday-depolarized and therefore most likely within a few hundred parsecs [91]. Foreground and background structures are difficult to distinguish when the shadowing interstellar material consists of magnetically organized dust structures with sub-parsec filaments and collapsing clouds. The Aquila Rift set of molecular clouds shadows the North Polar Spur X-ray emission [87, 88] but do not negate the optical polarization data that show a local origin for the Loop I magnetic field [74, 90].

Loop I and Loop IV are prominent high-latitude radio bubbles in galactic quadrants IV and I. Berkhuijsen et al. (1971, [6]) interpret these loops as supershells associated with evolved supernova remnants. The centers and diameters for Loop I and Loop IV are, respectively $\ell, b = 329^\circ \pm 1.5^\circ, +17.5^\circ \pm 3^\circ$, 116 ± 4 pc, and $\ell, b = 315^\circ \pm 3^\circ, +48.5^\circ \pm 1^\circ$, 39.5 ± 2 pc. The galactic bulge is 8.5 kpc beyond Loop I. Reynolds (1984, [71]) has shown that Loop IV is associated with a large hole in the distribution of nearby interstellar neutral hydrogen that coincides with an extended region of ionized hydrogen visible through Hα emission, and surrounding the hot variable star Spica (α Virginis, 80.8 ± 6.9 pc, B1V). The quasar 3C273 is viewed through the rim regions of Loop I and of Loop IV leading to complications in the interpretion of highly ionized gas in the X-ray spectrum of 3C273 [220]. Ultraviolet observations of the halo star HD 119608, located at 4.1 kpc and beyond Loops I and IV, show the bimodal velocity structure of an expanding shell [221]. The distance of HD 119608 and its foreground expanding shell indicate that the large-scale Loop I does not originate in the galactic center, while the coincidence of the HII region around Spica and Loop IV indicate that Loop IV is local.

3.6 The Orion-Eridanus Superbubble

The Orion region is the closest region that is actively forming high-mass stars. The activity of all the stars has combined to create the Orion-Eridanus bubble. At a distance of ~ 400 pc, it is a nearby expanding structure, explored over the entire wavelength range [169], that serves as a testbed for superbubble theories. A recent paper [170] has attempted to synthesize the previous data along with data collected from WISE and Planck to create a more complete model of the superbubble. The gen-

eral picture emerging from their investigations is that the bubble is larger and more complex than was previously assumed (Figure 5). It consists of a series of nested shells, the youngest of which, around the Orion Nebula Cluster, is less than 1 Myr old. Some other smaller bubbles triggered by ongoing activity are found around λ Ori, and the bubble GS206-17+13, most likely a stellar wind bubble approximately centered on the σ Ori cluster. In this model, Barnard's Loop is part of a complete bubble structure associated with a SNR that exploded about 0.3 Myr ago and then connected with the high-velocity gas detected in absorption studies towards this region. The expansion velocity of this structure is quite high, on the order of 100 km s^{-1}, again suggesting a recent origin. The outer shell of the Orion superbubble can be traced by observations of the intermediate velocity gas towards this region. In the west, some remnant of the neutral dense shell of the bubble can be seen, whereas towards the east the shell is completely ionized. High temperature ($\geq 10^6$ K) X-ray emitting gas is seen towards the west, while the gas temperature in the eastern interior is two orders of magnitude lower.

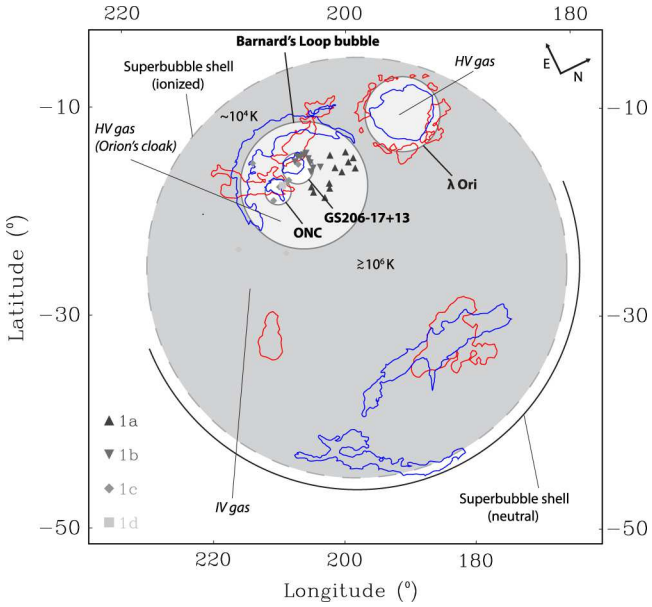


Fig. 5 Schematic of the Orion-Eridanus superbubble superbubble and several of its major components [170]: The Orion-Eridanus superbubble is shown together with the structures that trace this bubble. A superbubble formed from SNe in an old subpopulation of the Orion OB association and is traced by intermediate-velocity (IV) shocks [151, 168]. At lower galactic latitudes the superbubble is surrounded by a shell of neutral swept-up material (solid black line) that is not apparent in the opposite direction. Nested younger and smaller shells are shown (solid gray circles) such as the famous Barnard's Loop feature. See Ochsendorf et al. (2015, [170]) for more information.

The presence of various nested bubble structures suggests periods of episodic star formation in the Orion-Eridanus region. Instead of continuous input forming a single superbubble, each burst of star formation gave rise to different subgroups of stars that may locally ionize their environment, while stellar winds and the resulting SN explosions modify and tend to sweep up the surrounding medium into a bubble-like structure. The superbubble itself is probably 5-10 Myr old and was formed by a series of SNe that arose from stars in the Orion OB association. This model is supported further by the work of (Pon et al., 2016 [171]), who have attempted to fit a Kompaneets model of a superbubble expanding in an exponential atmosphere to this picture of the Orion-Eridanus bubble. They find morphologically consistent models with reasonable Galactic scale heights of 80 pc, provided that the bubble is oriented with the Eridanus side (at lower latitudes) further from the Sun than the Orion side.

4 Isotopic and Abundance Indicators of SN Activity

4.1 ^{60}Fe radioisotope Observations as Indicators of Nearby Supernovae

Measurements of ^{60}Fe in the terrestrial geological record provide an amazingly good indicator of encounters between supernovae ejecta and the heliosphere during the past several million years. ^{60}Fe is a radioactive isotope of iron with a half-life of 2.62 million years [172]. It is primarily produced in core-collapse of massive stars, which typically eject 10^{-5} to 10^{-4} $M_{\odot}$ of ^{60}Fe [173]. A small amount may be produced during the s-process before core-collapse, or by Asymptotic Giant Branch (AGB) stars. The important point is that there are no natural, terrestrial methods that produce ^{60}Fe ; therefore any terrestrial reservoirs of ^{60}Fe must be generally attributed to earlier deposition due to core-collapse supernovae (SNe), and can be considered as a signpost of the imprint of a nearby SN.

Using accelerator mass spectrometry, [174] found evidence of enhanced concentrations of ^{60}Fe radioactivity in deep ocean ferromanganese crust in the South Pacific. Further and better measurements led them to suggest the presence of a significant increase in the ^{60}Fe concentrations about 2.8 Myr ago [175], suggesting the presence of a SN explosion within a few tens of parsecs from the solar system. Fields et al. [176] combined the data with SNe nucleosynthesis models to refine the distance of a probable nearby SN to between 15 and 120 pc. Basu et al. (2007, [177]) posited an alternate theory, that the ^{60}Fe was due to the presence of micrometeorites trapped by the crust rather than injection by a SN, but many of their arguments were refuted by [178].

Recent work seems to further substantiate the SN origin of ^{60}Fe . Wallner et al. (2016, [179]) found that the ^{60}Fe signal was global by finding evidence of ^{60}Fe deposition in deep-sea archives from the Indian, Pacific and Atlantic oceans.

Furthermore, they find interstellar influx ^{60}Fe onto earth via dust grains between 1.7-3.2 Myr ago, with a second signal 6.5-8.7 Myr ago. They argue that these signals suggest recent massive star ejections, presumably supernova explosions, in the solar neighborhood within about 100 pc. Breitschwerdt et al. (2016, [180]) have modeled the SN explosions that created the Local Bubble based on the evolution and supernova rates in star clusters forming the Sco-Oph groups. They suggest that the ^{60}Fe signal is mainly due to two SNe that occurred 1.5 and 2.3 Myr ago, and between 90 and 100 pc distance from the solar system. The progenitor stars were about 9 $M_{\odot}$. These calculations assumed that the stars in the clusters were co-eval, which as pointed out by [81] and [82] may not be the case. This could result in a modification of the mass of the progenitor star. An 8-10 $M_{\odot}$ SN occurring 2.8 Myr ago, with material arriving at the Earth 2.2 Myr ago, was estimated by Fry et al. (2016, [181]).

Deep-ocean crusts are not the only evidence of ^{60}Fe concentrations. Fimiani et al. (2016, [182]) have confirmed earlier measurements [183, 184] that showed an excess of ^{60}Fe concentrations in lunar cores, which presumably originated from the same events that led to the ^{60}Fe deposition in ocean crusts. By measuring the concentration of ^{53}Mn in the same samples, they suggest that the ^{60}Fe is likely of SN origin, and that SN debris arrived on the moon about 2 Myr ago.

The Earth's microfossil record includes ^{60}Fe of biological origin. In 2013, Bishop et al. [185] analyzed Pacific ocean sediment drill cores. They were able to extract ^{60}Fe from magnetofossils and quantify abundances using a mass spectrometer. Further analysis recently reported by [186] confirms the direct detection of live ^{60}Fe atoms contained within secondary iron oxides, including magnetofossils, which are fossilized chains of magnetite crystals produced by magnetoactive bacteria. They suggest that the ^{60}Fe signal begins 2.6 - 2.8 Myr ago, peaks around 2.2 Myr earlier and terminates around 1.7 Myr earlier, consistent with the time periods deduced from other data such as deep-ocean crusts and lunar samples.

The composition of galactic cosmic rays reveals their origin as well as provides hints to the cosmic ray acceleration mechanisms. Using the Cosmic Ray Isotope Spectrometer (CRIS) instrument on the Advanced Composition Explorer (ACE) spacecraft, ^{60}Fe has been detected in cosmic rays of a few hundred MeV/nucleon [188]. The ^{60}Fe /^{56}Fe source ratio is $(7.5 \pm 2.9) \times 10^5$, which is consistent with that produced in massive stars. The detection of SN-produced ^{60}Fe in cosmic rays indicates that the time required for the acceleration and transport of the cosmic rays to earth cannot exceed the half-life of ^{60}Fe of 2.62 Myr. Consequently the distance from the source should be comparable to the distance that cosmic rays can diffuse over this time period, which they estimate to be less than 1 kpc. This is consistent with the existence of a SN within a kpc that exploded during the last 2.6 Myr.

4.2 Isotopes and the OB Association Origin of Galactic Cosmic Rays

Elemental abundances of galactic cosmic rays (GCRs) reveal both the origin and the acceleration mechanism of the GCRs. The largest differences between the isotopic composition of the GCRs and solar system values are found for the ratios ^{22}Ne /^{20}Ne , ^{12}C /^{16}O and ^{58}Fe /^{56}Fe . The ratio ^{22}Ne /^{20}Ne in GCRs is a factor of 5.3 ± 0.3 larger than the value in the solar wind [189]. Measurements of ^{22}Ne /^{20}Ne in the anomalous cosmic ray population (ACR) at lower energies, which form from interstellar neutrals that become charged while interacting with heliospheric plasma, show ratios consistent with solar values [190]. The enhanced ratio ^{22}Ne /^{20}Ne in GCRs suggests a source that includes contributions from the ejecta of massive stars. Binns et al. (2005, [189]) have shown that the ratio can be explained as resulting from a mixture of $\approx$20% massive star ejecta and wind material with $\sim$80% interstellar medium. In fact they further show that such an admixture could explain a range of isotope and element ratios for $Z \leq 28$ nuclei. Newer measurements [191] of abundances with $Z \geq 26$ are consistent with this, and indicate that GCRs have formed from a mixture of 19% ejecta from massive stars and 81% interstellar material with solar system composition. This means that the stellar winds and/or supernova have mixed with only about 4 times their ejected mass, which implies that the stellar source must not be mixing with too much interstellar material, suggesting the nearby presence of massive stars and/or supernovae.

Another isotopic constraint from GCRs is the lack of ^{59}Ni in cosmic rays. ^{59}Ni has a half-life of 76,000 years before it decays to ^{59}Co by electron capture. Once it is accelerated to high energy, the ^{59}Ni is stripped off electrons, and therefore cannot decay. Data from the CRIS experiment show a lack of ^{59}Ni in GCRs, indicating that the ^{59}Ni has decayed from the amount one would expect from a SN explosion [192]. Therefore Wiedenbeck et al. (1999, [192]) suggest that acceleration of the material took place at least 76,000 years after it was ejected. Thus while the ^{22}Ne /^{20}Ne ratio suggests that acceleration could not have taken place more than a few million years after the wind material was ejected (to avoid mixing too much interstellar medium material), the ^{59}Ni measurement shows that it must be at least 0.1 Myr after the SN explosion. It is possible that acceleration in superbubbles can satisfy both these constraints. However, it should be noted that a recent analysis by Neronov and Meynet (2016, [193]), taking the yield of ^{59}Ni from updated massive star models for stars up to 120 $M_{\odot}$, suggests a low ^{59}Ni yield compared to ^{59}Co , consistent with the CRIS experiments, which may remove the need for this constraint.

Balloon-born TIGER measurements of heavy GCRs $_{26}$Fe through $_{40}$Zi [194, 191] show that the abundances of $_{26}$Fe through $_{40}$Zi in the galactic cosmic ray population adhere to a pattern where the refractory elements in the GCR population are enhanced over volatile elements. Refractory elements in GCRs with energies of hundreds of MeV per nucleon to GeV per nucleon show a preferential acceleration of a factor of four over the acceleration of volatiles [191]. Epstein (1980, [195]) was one of the first to explain the high abundance of refractory elements in cosmic

rays, by suggesting that they were preferentially accelerated. Bibring and Cesarsky (1981, [196]) indicated that SN shocks can pick up particles from a suprathermal population produced by the destruction of dust grains. Ellison et al. (1997, [197]) produced the first detailed model explaining GCR abundances and isotopic ratios using interstellar grains that are accelerated to modest energies by SN shock waves. Grain destruction in the shock layer results from the thermal sputtering of particles from grain surfaces due to gas-grain collisions and grain shattering and vaporization during grain-grain collisions [198, 199, 200, 148]. Refractory elements show a well-known resilience against destruction. High condensation temperatures lead to refractory elements being injected into the shock at higher energies than volatiles, giving rise to the preferential acceleration of refractory elements in contrast to the volatiles that are accelerated in accordance with their mass-to-charge ratio (Ellison et al. 1997, [197]).

Signatures of a nearby supernova have been postulated in the locally observed cosmic ray spectrum. [187] have suggested that the excess of positrons and antiprotons above $\sim$20 GeV, and the discrepancy of slopes in the spectra of cosmic ray protons and heavier nuclei in the TeV-PeV energy range, can be explained as due to a nearby source, which was active about 2 Myr ago. This source injected about 2-3 $\times 10^{50}$ erg of energy in cosmic rays. The transient nature and overall energy budget suggest a SN origin, with an age equal to that given by the other indicators above.

4.3 ^{26}Al *as a Tracer of Massive Stars*

In 1999, Knodlseder [201] showed from an analysis of Comptel data that the 1.8 MeV gamma-ray line was closely correlated with the 53 GHz free-free emission in the Galaxy. 1.8 MeV gamma-rays are emitted during the radioactive decay of ^{26}Al, which has a half-life of about 0.7 Myr. The free-free emission arises from the ionized interstellar medium. He argued that this could be understood if massive stars are the source of ^{26}Al. Knodlseder et al. [202] showed that the correlation was also strong with other tracers of the young stellar population, which confirmed that the source of ^{26}Al was massive stars and supernovae.

Using spatial maps from the Comptel observatory to identify isolated regions of γ-ray emission, and the INTEGRAL γ-ray spectrometer to identify the γ-ray velocities, Diehl et al. (2010, [203]) identified a γ-ray source expanding toward the Sun at 137 ± 75 km s^{-1} from a 10°-radius region centered on the Upper-Scorpius (US) subgroup of the Sco-Cen Association. Given the 0.717 Myr half-life of ^{26}Al, this implies that the massive stars were born less than 10 Myr ago, thus indicating recent star formation. De Geus (1992, [80]) suggested that the proto-US cloud was compressed by an expanding shell from the Upper Centaurus-Lupus association ~ 4 Myr ago, igniting star formation. Since the velocity of the γ-ray source exceeds the ~ 10 km s^{-1} velocity of the HI shell around the US subgroup, Diehl et al. [203] have adopted the scenario where the high-velocity gas is stellar ejecta streaming into an adjacent preexisting cavity, and that deceleration occurred as the gas collided with

the preexisting walls of the bubble [203]. The young star clusters in a spiral arm will feed ^{26}Al ejecta into pre-existing HI supershell cavities that were left over from earlier star formation during passage of the previous spiral arm density wave [204].

5 Impact of Supernova on Heliosphere

Supernovae impact the heliosphere through the direct encounter of the heliosphere with the SN blast wave or ejecta, or modification of the ISM properties at the heliosphere. As discussed above, the Sun is traveling through the shell of the Loop I superbubble that resulted from stellar evolution in the ScoCen OB2 association. It was recognized long ago that extreme variations in the physical properties of interstellar material interacting with the solar system would probably affect the terrestrial climate [1, 205, 206, 207, 208, 209, 3]. These effects are mediated by the interaction between the heliosphere and interstellar medium [210, 207, 3, 208, 211, 212]. The 18 km s^{-1} motion of the solar system through the LSR and the 7–47 km s^{-1} LSR velocities of nearby interstellar clouds [121] lead to variations in the heliospheric boundary conditions over geological timescales of order $\leq$ 30 kyr [213]. Implications of our changing galactic environment are discussed in Scherer et al. (2006, [208]) and Frisch (2006, [209]).

The heliosphere configuration is governed by the relative pressures of the solar wind and interstellar material, including the dynamic ram pressure that increases non-linearly with the interaction velocity $\sim V^2$, and by interstellar ionizations since excluded ions and penetrating neutrals interact differently [210, 212]. Even a moderate increase in the relative velocities of the Sun and surrounding interstellar cloud from the present 25.4 km s^{-1} LIC velocity [133, 142] to 45 km s^{-1} (such as found for the cloud named "Vela" by Redfield and Linsky 2008, [122]) leads to a decrease of the heliopause distance by 34% percent from 104 AU to 69 AU [3]. Interactions between the heliosphere and an evolving superbubble at different velocities leads to different configurations for the heliosphere. Variations in the heliosphere-interstellar interactions also arise from variations in the solar magnetic activity cycle (e.g., [214, 215]).

The extreme example of the influence of our galaxy on the heliosphere would arise from the explosion of a supernova close to the Sun. The wind from the massive-star preceding a core-collapse supernova would, if close to the Sun, create a fully ionized environment for the heliosphere. The supernova explosion would first be noticed by an intense flux of UV/X-ray photons from the SN explosion itself that could ionize and heat the cloud around the heliosphere. A counter-intuitive result is that the flux of galactic cosmic rays at the Earth will increase for immersion of the heliosphere in a fully ionized plasma (Figure 7). Penetrating interstellar neutrals become ionized through charge-exchange, photoionization, and other processes [162] to create pickup ions that become accelerated to form anomalous cosmic rays [156]. The pickup ions that are trapped on the solar wind magnetic field lines mass-load the wind and increase turbulence that impedes the propagation of galactic cosmic rays to the inner heliosphere. Figure 7 shows that GCR fluxes in the inner helio-

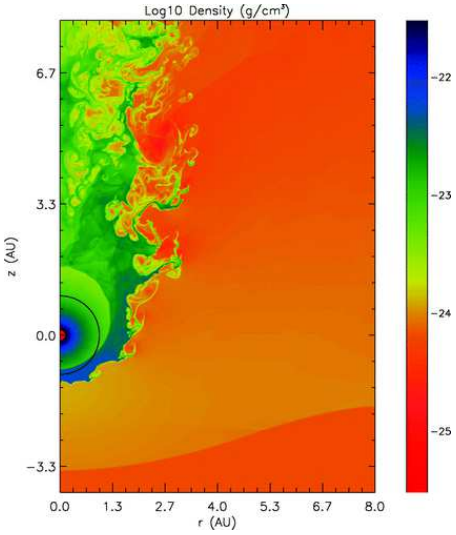


Fig. 6 One scenario showing the impact of a SNe blast wave on the heliosphere. A map of the logarithmic density of the heliosphere is shown after interaction with the shock from a supernova explosion 10 pc away for an explosion occurring in a tenuous unmagnetized low density cloud similar to the LIC. The Sun is located at the origin. Two shocks result, the innermost shock forms where the solar wind decelerates from a supersonic to a subsonic plasma, and the outer shock, the heliospheric bow shock, occurs where the blast wave becomes subsonic. The interface between the two fluids is marked by Kelvin-Helmholtz instabilities. In this model the SNR dominates the solar wind at 1 AU. See Fields et al. (2008, [216]) for additional information.

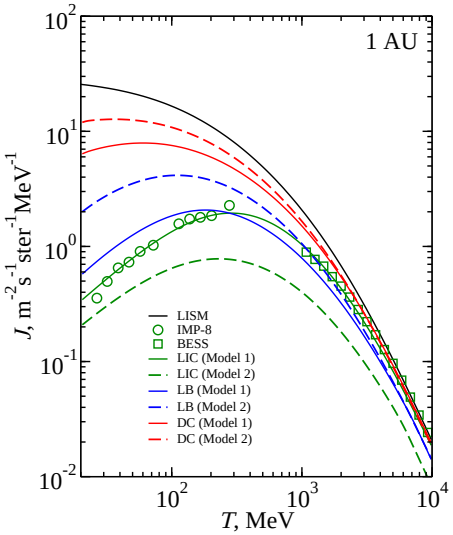


Fig. 7 Galactic cosmic ray fluxes at Earth for different solar environments. Higher GCR fluxes are found at the Earth when the Sun is immersed in a fully ionized hot plasma (blue lines) compared to for today's immersion of the Sun in the LIC (green lines). This effect arises from the charge-exchange between the interstellar neutrals and the solar wind that increases turbulence and the modulation of the GCR component through mass-loading. See Mueller et al. (2008, [217]) for more information.

sphere could increase by an order of magnitude if the surrounding interstellar cloud became fully ionized by a nearby supernova.

A blast wave from a nearby supernova would compress the heliosphere. Heliosphere multifluid models predict an encounter with a decelerated super bubble shell, at a velocity 100 km s^{-1} relative to the heliosphere, would shrink the heliopause to $\sim$ 14 AU for a warm tenuous cloud (8,000 K, $n \sim 0.8$ cm^{-3}) [3]. Numerical simulations show that a blast wave of thousands of km s^{-1} would sweep away the heliosphere, possibly leaving the Earth directly immersed in the supernova remnant. Fields et al. (2008, [216]) simulated a scenario for the heliosphere responding to a supernova that is located 8 pc away (Fig. 6). The interface between the solar wind and remnant plasma becomes highly unstable due to Kelvin-Helmholtz instabilities. These particular simulations do not explore a medium modified by the winds of the progenitor star (e.g. [39, 47, 43]), which could alter the scenario.

The proximity of active OB stars to the Sun could lead to an excess of photons at the time of shock breakout that would result in a potentially significant influence on the physical conditions of the interstellar medium that shapes the heliosphere. There is no a priori basis for assuming a constant radiation field at the Earth over the past $\sim$ 1 Myr. Slavin and Frisch (1996, [218]) have modeled the photon burst created by the supernova parent of the young Vela pulsar, $< 30,000$ years old and located at edge of the low density Local Bubble region in the near side of the Gum nebula, and suggested that the supernova may have contributed to the ionization of the interstellar cloud around the heliosphere. Recombination times for LIC-like gas at densities 0.1 cm^{-3} are $\sim 650,000$ years and longer if the gas is hotter. Possible sources of the ionizing radiation include γ-rays and the break-out of the supernova shock from the stellar atmosphere. Brakenridge(1981, [4]) concluded that radiation from a nearby supernova may have left isotopic signatures in the ^{14}C terrestrial record, and that the Vela supernova may explain a ^{14}C anomaly 15,000 years ago.

The photobiological effects of a supernova that occurred 2.5 Myr ago, at a distance of 50 pc, have been recently explored by [219]. They conclude that biological impacts due to increased UV irradiance by the nearby SN were not at a mass-extinction level, but could have contributed to changes in the abundances of various species. Such a conclusion is consistent with species turnover observed around the Pliocene-Pleistocene boundary.

6 Conclusions

The interstellar medium of the solar neighborhood within $\sim$ 500 pc has been shaped by the massive stars assigned to Gould's Belt in earlier studies. The nearest region of star formation is in the Scorpius-Centaurus Association where multiple supernovae have erupted during the past 15 Myr. Winds and supernova in these regions create bubbles and superbubbles that remix the interstellar medium over spatial scales of 500 pc. These bubbles are detected as filaments and loops of synchrotron emission arising from the compressed interstellar magnetic fields in the bubble walls and/or shells of HI gas swept up by the expanding bubbles. Two examples are the Loop I superbubble, which has expanded to the solar location, and the more distant Orion-Eridanus superbubble. The cluster of local interstellar clouds, as well as the ISM flowing through the heliosphere, display signatures of an origin inside of the rim of the Loop I superbubble, including the interstellar magnetic field direction and cloud velocities through the LSR. Cosmic ray isotopes trace the mixing of local interstellar material with the interstellar medium. The discovery of short-lived radio-isotopes in the geologic record indicate that the Earth has received material from supernovae occurring within the past $\sim$2 Myr. Heliosphere models show that the heliosphere is a sensitive barometer for interstellar pressures and would react dramatically to the explosion of a nearby supernova. A diversity of astrophysical and geological data are converging to allow new insights into the origin of interstellar material around the

Sun and to expand our perspective to include the relation between the heliosphere and the Milky Way galaxy.

Acknowledgments: PCF would like to thank NASA for the support of this research through the IBEX funding component of the NASA Explorer program, and through a grant from the Space Telescope Science Institute. VVD is grateful for support from NASA Emerging Worlds grant NNX15AH70G. His work on supernovae, circumstellar interaction and wind-blown bubbles has been supported over the years by NASA and the Chandra X-ray Center. VVD acknowledges useful discussions with the members of Team 351 at the ISSI in Bern, Switzerland, April 2016.

References

1. H. Shapley, J. Geology **29** (1921)
2. V. Florinski, G.P. Zank, in *Solar Journey: The Significance of Our Galactic Environment for the Heliosphere and Earth* (Springer, 2006), pp. 281–316
3. H.R. Müller, P.C. Frisch, V. Florinski, G.P. Zank, ApJ, **647**, 1491 (2006)
4. G.R. Brakenridge, Icarus, **46**, 81 (1981)
5. P.C. Frisch, B.G. Andersson, A. Berdyugin, V. Piirola, H.O. Funsten, A.M. Magalhaes, D.B. Seriacopi, D.J. McComas, N.A. Schwadron, J.D. Slavin, S.J. Wiktorowicz, ApJ, **805**, 60 (2015). DOI 10.1088/0004-637X/805/1/60
6. E.M. Berkhuijsen, C.G.T. Haslam, C.J. Salter, A&A., **14**, 252 (1971)
7. J.B. Rogerson, D.G. York, J.F. Drake, E.B. Jenkins, D.C. Morton, L. Spitzer, ApJ Lett., **181**, L110 (1973). DOI 10.1086/181196
8. S. Redfield, J.L. Linsky, ApJ, **613**, 1004 (2004)
9. P.C. Frisch, S. Redfield, J. Slavin, Ann. Rev. Astron. Astrophys., **49** (2011)
10. J.D. Slavin, P.C. Frisch, A&A., **491**, 53 (2008)
11. N.A. Schwadron, F. Allegrini, M. Bzowski, E.R. Christian, G.B. Crew, M. Dayeh, R. DeMajistre, P. Frisch, H.O. Funsten, S.A. Fuselier, K. Goodrich, M. Gruntman, P. Janzen, H. Kucharek, G. Livadiotis, D.J. McComas, E. Moebius, C. Prested, D. Reisenfeld, M. Reno, E. Roelof, J. Siegel, R. Vanderspek, ApJ, **731**, 56 (2011). DOI 10.1088/0004-637X/731/1/56
12. D.M. Meyer, J.T. Lauroesch, J.E.G. Peek, C. Heiles, ApJ, **752**, 119 (2012). DOI 10.1088/0004-637X/752/2/119
13. J.E.G. Peek, C. Heiles, K.M.G. Peek, D.M. Meyer, J.T. Lauroesch, ApJ, **735**, 129 (2011). DOI 10.1088/0004-637X/735/2/129
14. M. Salvati, A&A., **513**, A28+ (2010)
15. D.J. McComas, F. Allegrini, P. Bochsler, M. Bzowski, E.R. Christian, G.B. Crew, R. DeMajistre, H. Fahr, H. Fichtner, P.C. Frisch, H.O. Funsten, S.A. Fuselier, G. Gloeckler, M. Gruntman, J. Heerikhuisen, V. Izmodenov, P. Janzen, P. Knappenberger, S. Krimigis, H. Kucharek, M. Lee, G. Livadiotis, S. Livi, R.J. MacDowall, D. Mitchell, E. Möbius, T. Moore, N.V. Pogorelov, D. Reisenfeld, E. Roelof, L. Saul, N.A. Schwadron, P.W. Valek, R. Vanderspek, P. Wurz, G.P. Zank, Science, **326**, 959 (2009)
16. N.A. Schwadron, M. Bzowski, G.B. Crew, M. Gruntman, H. Fahr, H. Fichtner, P.C. Frisch, H.O. Funsten, S. Fuselier, J. Heerikhuisen, V. Izmodenov, H. Kucharek, M. Lee, G. Livadiotis, D.J. McComas, E. Moebius, T. Moore, J. Mukherjee, N.V. Pogorelov, C. Prested, D. Reisenfeld, E. Roelof, G.P. Zank, Science, **326**, 966 (2009)
17. H.O. Funsten, R. DeMajistre, P.C. Frisch, J. Heerikhuijsen, D.M. Higdon, P. Janzen, B. Larsen, G. Livadiotis, D.J. McComas, E. Möbius, C. Reese, D.B. Reisenfeld, N.A. Schwadron, E.J. Zirnstein, ApJ, **776**, 30 (2013)
18. J. Heerikhuisen, N.V. Pogorelov, G.P. Zank, G.B. Crew, P.C. Frisch, H.O. Funsten, P.H. Janzen, D.J. McComas, D.B. Reisenfeld, N.A. Schwadron, ApJ Lett., **708**, L126 (2010)

19. E.J. Zirnstein, J. Heerikhuisen, H.O. Funsten, G. Livadiotis, D.J. McComas, N.V. Pogorelov, ApJ Lett., **818**, L18 (2016). DOI 10.3847/2041-8205/818/1/L18
20. P.C. Frisch, A. Berdyugin, V. Piirola, A.M. Magalhaes, D.B. Seriacopi, S.J. Wiktorowicz, B.G. Andersson, H.O. Funsten, D.J. McComas, N.A. Schwadron, J.D. Slavin, A.J. Hanson, C.W. Fu, In preparation (2016)
21. C.A. Perrot, I.A. Grenier, A&A., **404**, 519 (2003). DOI 10.1051/0004-6361:20030477
22. I.A. Grenier, ArXiv Astrophysics e-prints (2004)
23. V.V. Bobylev, Astrophysics, **57**, 583 (2014). DOI 10.1007/s10511-014-9360-7
24. E.J. Alfaro, J. Cabrera-Cano, A.J. Delgado, ApJ, **378**, 106 (1991). DOI 10.1086/170410
25. R. Stothers, J.A. Frogel, AJ, **79**, 456 (1974)
26. V.V. Bobylev, A.T. Bajkova, Astronomy Letters, **40**, 783 (2014). DOI 10.1134/S1063773714120020
27. E.J. Alfaro, F. Elias, J. Cabrera-Caño, Ap&SS, **324**, 141 (2009). DOI 10.1007/s10509-009-0119-2
28. F. Elias, E.J. Alfaro, J. Cabrera-Caño, MNRAS, **397**, 2 (2009). DOI 10.1111/j.1365-2966.2009.14465.x
29. C. Heiles, ApJ, **229**, 533 (1979)
30. C. Heiles, ApJS, **55**, 585 (1984)
31. D.P. Cox, Ann. Rev. Astron. Astrophys., **43**, 337 (2005). DOI 10.1146/annurev.astro.43.072103.150615
32. C. Heiles, ApJ, **336**, 808 (1989)
33. J. Castor, R. McCray, R. Weaver, ApJ Lett., **200**, L107 (1975). DOI 10.1086/181908
34. R. Weaver, R. McCray, J. Castor, P. Shapiro, R. Moore, ApJ, **218**, 377 (1977). DOI 10.1086/155692
35. C.F. McKee, D. van Buren, B. Lazareff, ApJ Lett., **278**, L115 (1984). DOI 10.1086/184237
36. B.C. Koo, C.F. McKee, ApJ, **388**, 93 (1992). DOI 10.1086/171132
37. B.C. Koo, C.F. McKee, ApJ, **388**, 103 (1992). DOI 10.1086/171133
38. A.J. van Marle, Z. Meliani, A. Marcowith, A&A., **584**, A49 (2015). DOI 10.1051/0004-6361/201425230
39. G. Garcia-Segura, M.M. Mac Low, N. Langer, A&A., **305**, 229 (1996)
40. G. Garcia-Segura, N. Langer, M.M. Mac Low, A&A., **316**, 133 (1996)
41. T. Freyer, G. Hensler, H.W. Yorke, ApJ, **594**, 888 (2003). DOI 10.1086/376937
42. T. Freyer, G. Hensler, H.W. Yorke, ApJ, **638**, 262 (2006). DOI 10.1086/498734
43. V.V. Dwarkadas, ApJ, **667**, 226 (2007). DOI 10.1086/520670
44. G. Tenorio-Tagle, P. Bodenheimer, J. Franco, M. Rozyczka, MNRAS**244**, 563 (1990)
45. G. Tenorio-Tagle, M. Rozyczka, J. Franco, P. Bodenheimer, MNRAS, **251**, 318 (1991). DOI 10.1093/mnras/251.2.318
46. M. Rozyczka, G. Tenorio-Tagle, J. Franco, P. Bodenheimer, MNRAS**261**, 674 (1993). DOI 10.1093/mnras/261.3.674
47. V.V. Dwarkadas, ApJ, **630**, 892 (2005). DOI 10.1086/432109
48. A.J. van Marle, N. Smith, S.P. Owocki, B. van Veelen, MNRAS, **407**, 2305 (2010). DOI 10.1111/j.1365-2966.2010.16851.x
49. Y.H. Chu, R.A. Gruendl, M.A. Guerrero, in *Revista Mexicana de Astronomia y Astrofisica Conference Series*, *Revista Mexicana de Astronomia y Astrofisica, vol. 27*, vol. 15, ed. by J. Arthur, W.J. Henney (2003), *Revista Mexicana de Astronomia y Astrofisica, vol. 27*, vol. 15, pp. 62–67
50. Y.H. Chu, M.A. Guerrero, R.A. Gruendl, G. García-Segura, H.J. Wendker, ApJ, **599**, 1189 (2003). DOI 10.1086/379607
51. J.A. Toalá, M.A. Guerrero, Y.H. Chu, R.A. Gruendl, MNRAS, **446**, 1083 (2015). DOI 10.1093/mnras/stu2163
52. J.A. Toalá, M.A. Guerrero, Y.H. Chu, S.J. Arthur, D. Tafoya, R.A. Gruendl, MNRAS, **456**, 4305 (2016). DOI 10.1093/mnras/stv2819
53. J.A. Toalá, S.J. Arthur, ApJ, **737**, 100 (2011). DOI 10.1088/0004-637X/737/2/100
54. V.V. Dwarkadas, D.L. Rosenberg, High Energy Density Physics **9**, 226 (2013). DOI 10.1016/j.hedp.2012.12.003

55. V.V. Dwarkadas, D. Rosenberg, in *Wolf-Rayet Stars: Proceedings of an International Workshop held in Potsdam, Germany, 1-5 June 2015. Edited by Wolf-Rainer Hamann, Andreas Sander, Helge Todt. Universitätsverlag Potsdam, 2015., p.329-332*, ed. by W.R. Hamann, A. Sander, H. Todt (2015), pp. 329–332
56. M.M. Mac Low, R. McCray, ApJ, **324**, 776 (1988). DOI 10.1086/165936
57. M.M. Mac Low, R. McCray, M.L. Norman, ApJ, **337**, 141 (1989). DOI 10.1086/167094
58. N. Yadav, D. Mukherjee, P. Sharma, B.B. Nath, ArXiv e-prints, (2016)
59. M.J. Korpi, A. Brandenburg, A. Shukurov, I. Tuominen, A&A., **350**, 230 (1999)
60. J.M. Shull, in *Massive Stars: Their Lives in the Interstellar Medium*, *Astronomical Society of the Pacific Conference Series*, vol. 35, ed. by J.P. Cassinelli, E.B. Churchwell (1993), *Astronomical Society of the Pacific Conference Series*, vol. 35, p. 327
61. M.S. Oey, G. García-Segura, ApJ, **613**, 302 (2004). DOI 10.1086/421483
62. K.M. Ferriere, M. Mac Low, E.G. Zweibel, ApJ, **375**, 239 (1991)
63. H. Hanayama, K. Tomisaka, ApJ, **641**, 905 (2006). DOI 10.1086/500527
64. M.M. Mac Low, in *New Perspectives on the Interstellar Medium*, *Astronomical Society of the Pacific Conference Series*, vol. 168, ed. by A.R. Taylor, T.L. Landecker, G. Joncas (1999), *Astronomical Society of the Pacific Conference Series*, vol. 168, p. 303
65. R. Hanbury Brown, R.D. Davies, C. Hazard, The Observatory, **80**, 191 (1960)
66. R.D. Davies, MNRAS, **128**, 173 (1964). DOI 10.1093/mnras/128.2.173
67. E.M. Berkhuijsen, A&A., **14**, 359 (1971)
68. C.J. Salter, Bulletin of the Astronomical Society of India, **11**, 1 (1983)
69. C. Heiles, Y.. Chu, T.H. Troland, R.J. Reynolds, I. Yegingil, ApJ, **242**, 533 (1980)
70. M. Kun, in *Triggered Star Formation in a Turbulent ISM*, *IAU Symposium*, vol. 237, ed. by B.G. Elmegreen, J. Palous (2007), *IAU Symposium*, vol. 237, pp. 119–123. DOI 10.1017/S1743921307001329
71. R.J. Reynolds, in *NASA Conference Publication*, *NASA Conference Publication*, vol. 2345, ed. by Y. Kondo, F.C. Bruhweiler, B.D. Savage (1984), *NASA Conference Publication*, vol. 2345
72. M. Vidal, C. Dickinson, R.D. Davies, J.P. Leahy, MNRAS, **452**, 656 (2015). DOI 10.1093/mnras/stv1328
73. M. Wolleben, ApJ, **664**, 349 (2007). DOI 10.1086/518711
74. F.P. Santos, W. Corradi, W. Reis, ApJ, **728**, 104 (2011)
75. R.J. Egger, B. Aschenbach, A&A., **294**, L25 (1995)
76. C. Heiles, W.T. Reach, B.C. Koo, ApJ, **466**, 191 (1996)
77. E.J. de Geus, in *The Formation and Evolution of Star Clusters*, *Astronomical Society of the Pacific Conference Series*, vol. 13, ed. by K. Janes (1991), *Astronomical Society of the Pacific Conference Series*, vol. 13, pp. 40–54
78. I.A. Crawford, A&A., **247**, 183 (1991)
79. A. Blaauw, Ann. Rev. Astron. Astrophys., **2**, 213 (1964). DOI 10.1146/annurev.aa.02.090164.001241
80. E.J. de Geus, A&A., **262**, 258 (1992)
81. M J. Pecaut, E E. Mamajek, E. J. Bubar, ApJ, **746**, 154 (2012)
82. M J. Pecaut, E E. Mamajek, MNRAS, **461**, 794 (2016)
83. J. Maíz-Apellániz, ApJ Lett., **560**, L83 (2001)
84. P.C. Frisch, Nature, **293**, 377 (1981). DOI 10.1038/293377a0
85. D..C. Iwan, ApJ, **239**, 316 (1980)
86. D. Koutroumpa, R. Lallement, J.C. Raymond, V. Kharchenko, ApJ, **696**, 1517 (2009). DOI 10.1088/0004-637X/696/2/1517
87. Y. Sofue, MNRAS, **447**, 3824 (2015). DOI 10.1093/mnras/stu2661
88. R. Lallement, S. Snowden, K.D. Kuntz, T.M. Dame, D. Koutroumpa, I. Grenier, J.M. Casandjian, ArXiv e-prints, (2016)
89. M. Su, T.R. Slatyer, D.P. Finkbeiner, ApJ, **724**, 1044 (2010)
90. A. Berdyugin, V. Piirola, P. Teerikorpi, A&A., **561**, A24 (2014). DOI 10.1051/0004-6361/201322604

91. X.H. Sun, T.L. Landecker, B.M. Gaensler, E. Carretti, W. Reich, J.P. Leahy, N.M. McClure-Griffiths, R.M. Crocker, M. Wolleben, M. Haverkorn, K.A. Douglas, A.D. Gray, ApJ, **811**, 40 (2015). DOI 10.1088/0004-637X/811/1/40
92. C.S. Bowyer, G.B. Field, J.F. Mack, Nature, **217**, 32 (1968)
93. D. McCammon, D.N. Burrows, W.T. Sanders, W.L. Kraushaar, ApJ, **269**, 107 (1983)
94. F.O. Williamson, W.T. Sanders, W.L. Kraushaar, D. McCammon, R. Borken, A.N. Bunner, ApJ Lett., **193**, L133 (1974). DOI 10.1086/181649
95. W.T. Sanders, W.L. Kraushaar, J.A. Nousek, P.M. Fried, ApJ Lett., **217**, L87 (1977). DOI 10.1086/182545
96. D.P. Cox, R.J. Reynolds, Ann. Rev. Astron. Astrophys., **25**, 303 (1987). DOI 10.1146/annurev.aa.25.090187.001511
97. D. McCammon, W.T. Sanders, Ann. Rev. Astron. Astrophys., **28**, 657 (1990). DOI 10.1146/annurev.aa.28.090190.003301
98. N. Gehrels, C.M. Laird, C.H. Jackman, J.K. Cannizzo, B.J. Mattson, W. Chen, ApJ, **585**, 1169 (2003)
99. P.C. Frisch, Nature, **364**, 395 (1993)
100. V.V. Smith, K. Cunha, B. Plez, A&A., **281**, L41 (1994)
101. L.J. Pellizza, R.P. Mignani, I.A. Grenier, I.F. @ Mirabel, A&A., **435**, 625 (2005)
102. D.P. Cox, B.W. Smith, ApJ Lett., **189**, L105 (1974). DOI 10.1086/181476
103. N. Tetzlaff, G. Torres, R. Neuhäuser, M.M. Hohle, MNRAS, **435**, 879 (2013). DOI 10.1093/mnras/stt1358
104. R.K. Smith, D.P. Cox, ApJS, **134**, 283 (2001). DOI 10.1086/320850
105. B.Y. Welsh, R.L. Shelton, Ap&SS, **323**, 1 (2009). DOI 10.1007/s10509-009-0053-3
106. B. Fuchs, D. Breitschwerdt, M.A. de Avillez, C. Dettbarn, C. Flynn, MNRAS, **373**, 993 (2006). DOI 10.1111/j.1365-2966.2006.11044.x
107. M.A. de Avillez, D. Breitschwerdt, A&A., **539**, L1 (2012). DOI 10.1051/0004-6361/201117172
108. T.E. Cravens, I.P. Robertson, S.L. Snowden, J. Geophys. Res., **106**, 24883 (2001)
109. K.D. Kuntz, Y.M. Collado-Vega, M.R. Collier, H.K. Connor, T.E. Cravens, D. Koutroumpa, F.S. Porter, I.P. Robertson, D.G. Sibeck, S.L. Snowden, N.E. Thomas, B.M. Walsh, ApJ, **808**, 143 (2015). DOI 10.1088/0004-637X/808/2/143
110. P.C. Frisch, M. Bzowski, E. Grün, V. Izmodenov, H. Krüger, J.L. Linsky, D.J. McComas, E. Möbius, S. Redfield, N. Schwadron, R.R. Shelton, J.D. Slavin, B.E. Wood, Space Sci. Rev., **146**, 235 (2009)
111. R.K. Smith, A.R. Foster, R.J. Edgar, N.S. Brickhouse, ApJ, **787**, 77 (2014). DOI 10.1088/0004-637X/787/1/77
112. S.L. Snowden, C. Heiles, D. Koutroumpa, K.D. Kuntz, R. Lallement, D. McCammon, J.E.G. Peek, ApJ, **806**, 119 (2015). DOI 10.1088/0004-637X/806/1/119
113. S.L. Snowden, D. Koutroumpa, K.D. Kuntz, R. Lallement, L. Puspitarini, ApJ, **806**, 120 (2015). DOI 10.1088/0004-637X/806/1/120
114. C. Nehmé, C. Gry, F. Boulanger, J. Le Bourlot, G. Pineau Des Forêts, E. Falgarone, A&A., **483**, 471 (2008). DOI 10.1051/0004-6361:20078373
115. C. Gry, C. Nehmé, F. Boulanger, J. Lebourlot, G.P. Des Forêts, E. Falgarone, in *American Institute of Physics Conference Series*, *American Institute of Physics Conference Series*, vol. 1156, ed. by R.K. Smith, S.L. Snowden, K.D. Kuntz (2009), *American Institute of Physics Conference Series*, vol. 1156, pp. 218–222. DOI 10.1063/1.3211817
116. D.P. Cox, L. Helenius, ApJ, **583**, 205 (2003)
117. T.A.T. Spoelstra, A&A., **21**, 61 (1972)
118. E.M. Berkhuijsen, A&A., **24**, 143 (1973)
119. P.C. Frisch, ApJ, **714**, 1679 (2010). DOI 10.1088/0004-637X/714/2/1679
120. C. Heiles, ApJ, **498**, 689 (1998)
121. P.C. Frisch, N.A. Schwadron, in *Outstanding Problems in Heliophysics: From Coronal Heating to the Edge of the Heliosphere*, *Astronomical Society of the Pacific Conference Series*, vol. 484, ed. by Q. Hu, G.P. Zank (2014), *Astronomical Society of the Pacific Conference Series*, vol. 484, p. 42

122. S. Redfield, J.L. Linsky, ApJ, **673**, 283 (2008)
123. R.M. Crutcher, ApJ, **254**, 82 (1982)
124. P. Frisch, D.G. York, in *The Galaxy and the Solar System*, (University of Arizona Press, 1986), pp. 83–100
125. M. Bzowski, Acta Astronomica, **38**, 443 (1988)
126. P.C. Frisch, L. Grodnicki, D.E. Welty, ApJ, **574**, 834 (2002)
127. C. Gry, E.B. Jenkins, A&A., **567**, A58 (2014). DOI 10.1051/0004-6361/201323342
128. G.H. Herbig, Zeitschrift Astrophysics, **68**, 243 (1968)
129. R. Lallement, A. Vidal-Madjar, R. Ferlet, A&A., **168**, 225 (1986)
130. R. Lallement, P. Bertin, A&A., **266**, 479 (1992)
131. P.C. Frisch, ApJ, **593**, 868 (2003)
132. M.A. Kubiak, P. Swaczyna, M. Bzowski, J.M. Sokół, S.A. Fuselier, A. Galli, D. Heirtzler, H. Kucharek, T.W. Leonard, D.J. McComas, E. Möbius, J. Park, N.A. Schwadron, P. Wurz, ApJS, **223**, 25 (2016). DOI 10.3847/0067-0049/223/2/25
133. N.A. Schwadron, E. Moebius, T. Leonard, S.A. Fuselier, D.J. McComas, D. Heirtzler, H. Kucharek, F. Rahmanifard, M. Bzowski, M.A. Kubiak, J. Sokol, P. Swaczyna, P. Frisch, ApJS, **220**, 25 (2015). DOI 10.1088/0067-0049/220/2/25
134. P.C. Frisch, J.M. Dorschner, J. Geiss, J.M. Greenberg, E. Grün, M. Landgraf, P. Hoppe, A.P. Jones, W. Krätschmer, T.J. Linde, G.E. Morfill, W. Reach, J.D. Slavin, J. Svestka, A.N. Witt, G.P. Zank, ApJ, **525**, 492 (1999)
135. H. Kimura, I. Mann, E.K. Jessberger, ApJ, **582**, 846 (2003)
136. P.C. Frisch, ApJ, **227**, 474 (1979)
137. B.G. Andersson, A. Lazarian, J.E. Vaillancourt, Ann. Rev. Astron. Astrophys., **53**, 501 (2015). DOI 10.1146/annurev-astro-082214-122414
138. D.J. McComas, W.S. Lewis, N.A. Schwadron, Reviews of Geophysics, **52**, 118 (2014). DOI 10.1002/2013RG000438
139. N.A. Schwadron, D.J. McComas, ApJ, **764**, 92 (2013). DOI 10.1088/0004-637X/764/1/92
140. E. Möbius, P. Bochsler, M. Bzowski, G.B. Crew, H.O. Funsten, S.A. Fuselier, A. Ghielmetti, D. Heirtzler, V.V. Izmodenov, M. Kubiak, H. Kucharek, M.A. Lee, T. Leonard, D.J. McComas, L. Petersen, L. Saul, J.A. Scheer, N. Schwadron, M. Witte, P. Wurz, Science **326**, 969 (2009). DOI 10.1126/science.1180971
141. N.A. Schwadron, E. Moebius, H. Kucharek, M.A. Lee, J. French, L. Saul, P. Wurz, M. Bzowski, S.A. Fuselier, G. Livadiotis, D.J. McComas, P. Frisch, M. Gruntman, H.R. Mueller, ApJ, **775**, 86 (2013). DOI 10.1088/0004-637X/775/2/86
142. D.J. McComas, M. Bzowski, P. Frisch, S.A. Fuselier, M.A. Kubiak, H. Kucharek, T. Leonard, E. Möbius, N.A. Schwadron, J.M. Sokół, P. Swaczyna, M. Witte, ApJ, **801**, 28 (2015). DOI 10.1088/0004-637X/801/1/28
143. D.S. Ebel, J. Geophys. Res., **105**, 10363 (2000)
144. P. Routly, J. Spitzer, L., ApJ, **115**, 227 (1952)
145. L. Spitzer, Comments on Astrophysics, **6**, 177 (1976)
146. K.R. Sembach, A.C. Danks, A&A., **289**, 539 (1994)
147. R.S. Siluk, J. Silk, ApJ, **192**, 51 (1974)
148. A.P. Jones, A. Tielens, D.J. Hollenbach, ApJ**469**, 740 (1996)
149. J.D. Slavin, E. Dwek, A.P. Jones, ApJ, **803**, 7 (2015). DOI 10.1088/0004-637X/803/1/7
150. E.B. Jenkins, ApJ, **700**, 1299 (2009)
151. D.E. Welty, L.M. Hobbs, J.T. Lauroesch, D.C. Morton, L. Spitzer, D.G. York, ApJS, **124**, 465 (1999)
152. D.J. McComas, M. Bzowski, S.A. Fuselier, P.C. Frisch, A. Galli, V.V. Izmodenov, O.A. Katushkina, M.A. Kubiak, M.A. Lee, T.W. Leonard, E. Möbius, J. Park, N.A. Schwadron, J.M. Sokół, P. Swaczyna, B.E. Wood, P. Wurz, ApJS, **220**, 22 (2015). DOI 10.1088/0067-0049/220/2/22
153. V.J. Sterken, P. Strub, H. Krüger, R. von Steiger, P. Frisch, ApJ, **812**, 141 (2015)
154. N. Altobelli, F. Postberg, et al., Science, **352**, 6283 (2016). DOI 10.1126/science.aac6397

155. N.A. Schwadron, F.C. Adams, E.R. Christian, P. Desiati, P. Frisch, H.O. Funsten, J.R. Jokipii, D.J. McComas, E. Moebius, G.P. Zank, Science **343**, 988 (2014). DOI 10.1126/science.1245026
156. L.A. Fisk, B. Kozlovsky, R. Ramaty, ApJ, **190**, L35 (1974)
157. G. Gloeckler, L. Fisk, Space Sci. Rev., **27**, 489 (2007)
158. M. Witte, A&A., **426**, 835 (2004). DOI 10.1051/0004-6361:20035956
159. A.C. Cummings, E.C. Stone, C.D. Steenberg, ApJ, **578**, 194 (2002)
160. P.C. Frisch, Space Sci. Rev., **72**, 499 (1995)
161. B. Wolff, D. Koester, R. Lallement, A&A., **346**, 969 (1999)
162. M. Bzowski, J.M. Sokół, M.A. Kubiak, H. Kucharek, A&A., **557**, A50 (2013). DOI 10.1051/0004-6361/201321700
163. J. Park, H. Kucharek, E.e.a. Möbius, ApJ, **795**, 97 (2014)
164. J. Park, H. Kucharek, E. Möbius, A. Galli, G. Livadiotis, S.A. Fuselier, D.J. McComas, ApJS, **220**, 34 (2015). DOI 10.1088/0067-0049/220/2/34
165. N.A. Schwadron, E. Möbius, D.J. McComas, P. Bochsler, M. Bzowski, S.A. Fuselier, G. Livadiotis, P. Frisch, H.R. Müller, D. Heirtzler, H. Kucharek, M.A. Lee, ApJ, **828**, 81 (2016). DOI 10.3847/0004-637X/828/2/81
166. J.D. Slavin, ApJ, **346**, 718 (1989)
167. J.D. Slavin, P.C. Frisch, ApJ, **565**, 364 (2002)
168. D.E. Welty, E.B. Jenkins, J.C. Raymond, C. Mallouris, D.G. York, ApJ, **579**, 304 (2002)
169. C. Heiles, L.M. Haffner, R.J. Reynolds, in *New Perspectives on the Interstellar Medium*, *Astronomical Society of the Pacific Conference Series*, vol. 168, ed. by A.R. Taylor, T.L. Landecker, G. Joncas (1999), *Astronomical Society of the Pacific Conference Series*, vol. 168, p. 211
170. B.B. Ochsendorf, A.G.A. Brown, J. Bally, A.G.G.M. Tielens, ApJ, **808**, 111 (2015). DOI 10.1088/0004-637X/808/2/111
171. A. Pon, B.B. Ochsendorf, J. Alves, J. Bally, S. Basu, A.G.G.M. Tielens, ApJ, **827**, 42 (2016). DOI 10.3847/0004-637X/827/1/42
172. G. Rugel, T. Faestermann, K. Knie, G. Korschinek, M. Poutivtsev, D. Schumann, N. Kivel, I. Günther-Leopold, R. Weinreich, M. Wohlmuther, Physical Review Letters, **103**(7), 072502 (2009). DOI 10.1103/PhysRevLett.103.072502
173. M. Limongi, A. Chieffi, ApJ, **592**, 404 (2003). DOI 10.1086/375703
174. K. Knie, G. Korschinek, T. Faestermann, C. Wallner, J. Scholten, W. Hillebrandt, Physical Review Letters **83**, 18 (1999). DOI 10.1103/PhysRevLett.83.18
175. K. Knie, G. Korschinek, T. Faestermann, E.A. Dorfi, G. Rugel, A. Wallner, Physical Review Letters, **93**(17), 171103 (2004). DOI 10.1103/PhysRevLett.93.171103
176. B.D. Fields, K.A. Hochmuth, J. Ellis, ApJ, **621**, 902 (2005). DOI 10.1086/427797
177. S. Basu, F.M. Stuart, C. Schnabel, V. Klemm, Physical Review Letters, **98**(14), 141103 (2007). DOI 10.1103/PhysRevLett.98.141103
178. C. Fitoussi, G.M. Raisbeck, K. Knie, G. Korschinek, T. Faestermann, S. Goriely, D. Lunney, M. Poutivtsev, G. Rugel, C. Waelbroeck, A. Wallner, Physical Review Letters **101**(12), 121101 (2008). DOI 10.1103/PhysRevLett.101.121101
179. A. Wallner, J. Feige, N. Kinoshita, M. Paul, L.K. Fifield, R. Golser, M. Honda, U. Linnemann, H. Matsuzaki, S. Merchel, G. Rugel, S.G. Tims, P. Steier, T. Yamagata, S.R. Winkler, Nature, **532**, 69 (2016). DOI 10.1038/nature17196
180. D. Breitschwerdt, J. Feige, M.M. Schulreich, M.A.D. Avillez, C. Dettbarn, B. Fuchs, Nature, **532**, 73 (2016). DOI 10.1038/nature17424
181. B.J. Fry, B.D. Fields, J.R. Ellis, ApJ, **827**, 48 (2016). DOI 10.3847/0004-637X/827/1/48
182. L. Fimiani, D.L. Cook, T. Faestermann, J.M. Gómez-Guzmán, K. Hain, G. Herzog, K. Knie, G. Korschinek, P. Ludwig, J. Park, R.C. Reedy, G. Rugel, Physical Review Letters, **116**(15), 151104 (2016). DOI 10.1103/PhysRevLett.116.151104
183. D.L. Cook, E. Berger, T. Faestermann, G.F. Herzog, K. Knie, G. Korschinek, M. Poutivtsev, G. Rugel, F. Serefiddin, in *Lunar and Planetary Science Conference*, *Lunar and Planetary Inst. Technical Report*, vol. 40 (2009), *Lunar and Planetary Inst. Technical Report*, vol. 40, p. 1129

184. L. Fimiani, D.L. Cook, T. Faestermann, J.M. Gomez Guzman, K. Hain, G.F. Herzog, G. Korschinek, B. Ligon, P. Ludwig, J. Park, R.C. Reedy, G. Rugel, in *Lunar and Planetary Science Conference*, *Lunar and Planetary Inst. Technical Report*, vol. 43 (2012), *Lunar and Planetary Inst. Technical Report*, vol. 43, p. 1279
185. S. Bishop, P. Ludwig, R. Egli, V. Chernenko, T. Frederichs, S. Merchel, G. Rugel, in *APS April Meeting Abstracts* (2013)
186. P. Ludwig, S. Bishop, R. Eglib, V.e.a. Chernenkoa, PNAS, **113**, 9232 (2016). DOI 10.1073/pnas.1601040113
187. M. Kachelriess, A. Neronov, and D. V. Semikoz, PRL, **115**, 181103 (2015) DOI 10.1073/pnas.1601040113
188. W.R. Binns, M.H. Israel, E.R. Christian, A.C. Cummings, G.A. de Nolfo, K.A. Lave, R.A. Leske, R.A. Mewaldt, E.C. Stone, T.T. von Rosenvinge, M.E. Wiedenbeck, Science, **352**, 677 (2016). DOI 10.1126/science.aad6004
189. W.R. Binns, M.E. Wiedenbeck, M. Arnould, A.C. Cummings, J.S. George, S. Goriely, M.H. Israel, R.A. Leske, R.A. Mewaldt, G. Meynet, L.M. Scott, E.C. Stone, T.T. von Rosenvinge, ApJ, **634**, 351 (2005). DOI 10.1086/496959
190. R.A. Leske, in *26th International Cosmic Ray Conference, ICRC XXVI*, *American Institute of Physics Conference Series*, vol. 516, ed. by B.L. Dingus, D.B. Kieda, M.H. Salamon (2000), *American Institute of Physics Conference Series*, vol. 516, pp. 274–282. DOI 10.1063/1.1291481
191. R.P. Murphy, M. Sasaki, W.R. Binns, T.J. Brandt, T. Hams, M.H. Israel, A.W. Labrador, J.T. Link, R.A. Mewaldt, J.W. Mitchell, B.F. Rauch, K. Sakai, E.C. Stone, C.J. Waddington, N.E. Walsh, J.E. Ward, M.E. Wiedenbeck, ArXiv e-prints, (2016)
192. M.E. Wiedenbeck, W.R. Binns, E.R. Christian, A.C. Cummings, B.L. Dougherty, P.L. Hink, J. Klarmann, R.A. Leske, M. Lijowski, R.A. Mewaldt, E.C. Stone, M.R. Thayer, T.T. von Rosenvinge, N.E. Yanasak, ApJ Lett., **523**, L61 (1999). DOI 10.1086/312242
193. A. Neronov, G. Meynet, A&A., **588**, A86 (2016). DOI 10.1051/0004-6361/201527762
194. B.F. Rauch, J.T. Link, K. Lodders, M.H. Israel, L.M. Barbier, W.R. Binns, E.R. Christian, J.R. Cummings, G.A. de Nolfo, S. Geier, R.A. Mewaldt, J.W. Mitchell, S.M. Schindler, L.M. Scott, E.C. Stone, R.E. Streitmatter, C.J. Waddington, M.E. Wiedenbeck, ApJ, **697**, 2083 (2009). DOI 10.1088/0004-637X/697/2/2083
195. R.I. Epstein, MNRAS, **193**, 723 (1980). DOI 10.1093/mnras/193.4.723
196. J.P. Bibring, C.J. Cesarsky, International Cosmic Ray Conference, **2**, 289 (1981)
197. D.C. Ellison, L.O. Drury, J. Meyer, ApJ, **487**, 197 (1997)
198. M.J. Barlow, J. Silk, ApJ Lett., **211**, L83 (1977). DOI 10.1086/182346
199. B.T. Draine, E.E. Salpeter, ApJ, **231**, 438 (1979)
200. A.P. Jones, A.G.G.M. Tielens, D.J. Hollenbach, C.F. McKee, ApJ**433**, 797 (1994)
201. J. Knödlseder, ApJ, **510**, 915 (1999). DOI 10.1086/306601
202. J. Knödlseder, K. Bennett, H. Bloemen, R. Diehl, W. Hermsen, U. Oberlack, J. Ryan, V. Schönfelder, P. von Ballmoos, A&A., **344**, 68 (1999)
203. R. Diehl, M.G. Lang, P. Martin, H. Ohlendorf, T. Preibisch, R. Voss, P. Jean, J.P. Roques, P. von Ballmoos, W. Wang, A&A., **522**, A51 (2010). DOI 10.1051/0004-6361/201014302
204. M.G.H. Krause, R. Diehl, Y. Bagetakos, E. Brinks, A. Burkert, O. Gerhard, J. Greiner, K. Kretschmer, T. Siegert, A&A., **578**, A113 (2015). DOI 10.1051/0004-6361/201525847
205. F. Hoyle, R.A. Lyttleton, Proceedings of the Cambridge Philosophical Society **35**, 405 (1939). DOI 10.1017/S0305004100021150
206. D.H. Clark, W.H. McCrea, F.R. Stephenson, Nature, **265**, 318 (1977)
207. P.C. Frisch, ApJ, **407**, 198 (1993)
208. K. Scherer, H. Fichtner, T. Borrmann, J. Beer, L. Desorgher, E. Flükiger, H.J. Fahr, S.E.S. Ferreira, U.W. Langner, M.S. Potgieter, B. Heber, J. Masarik, N. Shaviv, J. Veizer, Space Sci. Rev., **127**, 327 (2006). DOI 10.1007/s11214-006-9126-6
209. P.C. Frisch, *Solar Journey: The Significance of Our Galactic Environment for the Heliosphere and Earth,* (Springer, 2006)
210. T.E. Holzer, Ann. Rev. Astron. Astrophys., **27**, 199 (1989)

211. G.P. Zank, P.C. Frisch, ApJ, **518**, 965 (1999)
212. G.P. Zank, Ann. Rev. Astron. Astrophys., **53**, 449 (2015). DOI 10.1146/annurev-astro-082214-122254
213. P.C. Frisch, H.R. Mueller, Space Sci. Rev., pp. 130–+ (2011). DOI 10.1007/s11214-011-9776-x
214. H. Washimi, T. Tanaka, Advances in Space Research, **23**, 551 (1999)
215. N.V. Pogorelov, S.T. Suess, S.N. Borovikov, R.W. Ebert, D.J. McComas, G.P. Zank, ApJ, **772**, 2 (2013). DOI 10.1088/0004-637X/772/1/2
216. B.D. Fields, T. Athanassiadou, S.R. Johnson, ApJ, **678**, 549-562 (2008). DOI 10.1086/523622
217. H.R. Müller, P.C. Frisch, B.D. Fields, G.P. Zank, Space Sci. Rev., p. 163 (2008)
218. J.D. Slavin, P.C. Frisch, Space Sci. Rev., **78**, 223 (1996)
219. B. C. Thomas, Astrobiology, arXiv:1711.00410
220. T. Fang, X. Jiang, ApJ Lett.**785**, L24 (2014). DOI 10.1088/2041-8205/785/2/L24
221. K.R. Sembach, B.D. Savage, T.M. Tripp, ApJ**480**, 216 (1997). DOI 10.1086/303956